Bioactive Materials 16 (2022) 472–484

Contents lists available at ScienceDirect

Bioactive Materials

journal homepage: www.keaipublishing.com/en/journals/bioactive-materials

Shear-responsive boundary-lubricated hydrogels attenuate osteoarthritis

Yiting Lei [a,1], Xingkuan Wang [b,1], Junyi Liao [a,1], Jieliang Shen [a], Yuling Li [b], Zhengwei Cai [c], Ning Hu [a], Xiaoji Luo [a,*], Wenguo Cui [c,**], Wei Huang [a,***]

[a] Department of Orthopedics, The First Affiliated Hospital of Chongqing Medical University, Orthopedic Laboratory of Chongqing Medical University, No.1 Youyi Road, Yuzhong District, Chongqing, 400016, PR China
[b] Department of Orthopaedics, Affiliated Hospital of North Sichuan Medical College, No. 1 the South of Maoyuan Road, Nanchong, Sichuan, 637000, PR China
[c] Department of Orthopaedics, Shanghai Key Laboratory for Prevention and Treatment of Bone and Joint Diseases, Shanghai Institute of Traumatology and Orthopaedics, Ruijin Hospital, Shanghai Jiao Tong University School of Medicine, 197 Ruijin 2nd Road, Shanghai, 200025, PR China

ARTICLE INFO

Keywords:
Boundary lubrication
Injectable hydrogels
Shear-responsive
Liposomes
Osteoarthritis

ABSTRACT

Lipid-based boundary layers formed on liposome-containing hydrogels can facilitate lubrication. However, these boundary layers can be damaged by shear, resulting in decreased lubrication. Here, a shear-responsive boundary-lubricated drug-loaded hydrogel is created by incorporating celecoxib (CLX)-loaded liposomes within dynamic covalent bond-based hyaluronic acid (HA) hydrogels (CLX@Lipo@HA-gel). The dynamic cross-linked network enables the hydrogel to get restructured in response to shear, and the HA matrix allows the accumulation of internal liposome microreservoirs on the sliding surfaces, which results in the formation of boundary layers to provide stable lubrication. Moreover, hydration shells formed surrounding the hydrogel can retard the degradation process, thus helping in sustaining lubrication. Furthermore, in vitro and in vivo experiments found that CLX@Lipo@HA-gels can maintain anabolic-catabolic balance, alleviate cartilage wear, and attenuate osteoarthritis progression by delivering CLX and shear-responsive boundary lubrication. Overall, CLX@Lipo@HA-gels can serve as shear-responsive boundary lubricants and drug-delivery vehicles to alleviate friction-related diseases like osteoarthritis.

1. Introduction

Inadequate lubrication in biological surfaces (e.g., diarthrodial joints or skin) can cause a wide range of friction-related diseases (e.g., osteoarthritis or xeroderma) [1,2]. Hydrogels are soft materials with a three-dimensional network structure that can retain plenty of water [3,4]. During sliding, the fluid film formed on the surface of hydrogels can prevent direct contact between sliding surfaces, thus reducing wear and friction forces [5]. Hydrogels are widely used in the area of biolubrication because of their desirable biocompatibility. However, most injectable hydrogels are mechanically weak and become severely deformed under high-pressure conditions (e.g., joint surface) [6]. In this case, water on the surface and inside the hydrogels can be squeezed out, which may decrease the effect of fluid film lubrication [7]. Therefore, measures to improve the lubrication performance of hydrogels in joints are an urgent necessity.

Introducing boundary layers on hydrogels can combine water molecules to form hydration shells that cannot be easily squeezed out at physiological pressures and provide efficient lubrication [8,9]. As the main lubricating macromolecules of synovial fluid [10], proteoglycan 4 and hyaluronic acid (HA) have each demonstrated boundary-lubricating ability [11]. In addition, they can also interact with each other and play a synergistic role in boundary lubrication [12]. Recently, as another major lubricating constituent of synovial fluid; phospholipids (usually in the form of liposomes) have received increasing attention in the field of boundary lubrication [11,13]. Lin et al. fabricated a novel boundary-lubricated hydrogel by incorporating hydrogenated soy phosphatidylcholine (HSPC) liposomes to form microreservoirs throughout the gel bulk [14]. However, these hydrogels, such as poly (hydroxyethylmethacrylate) hydrogel, are formed by permanent

Peer review under responsibility of KeAi Communications Co., Ltd.
* Corresponding author.
** Corresponding author.
*** Corresponding author.
E-mail addresses: cy2982@163.com (X. Luo), wgcui80@hotmail.com (W. Cui), huangw511@163.com (W. Huang).
[1] The authors contributed equally to this work.

https://doi.org/10.1016/j.bioactmat.2022.02.016
Received 24 December 2021; Received in revised form 20 January 2022; Accepted 12 February 2022
Available online 20 February 2022

cross-linking, and the network structure cannot be changed once the gel formation is completed. As a result, the liposome microreservoirs are firmly anchored within the hydrogel networks and cannot migrate in response to external stimuli. In addition to pressure, shear is another crucial factor to be considered in joint lubrication [15]. Once the boundary layers get damaged because of shear [16], these hydrogels cannot expose their internal liposome microreservoirs until the outer surfaces are worn off, leading to unstable lubrication. Thus, developing shear-responsive hydrogels that can restructure according to shear, and expose internal liposome microreservoirs on the interface to form stable boundary layers will be of great significance to extend the application of hydrogels.

Dynamic covalent bonds, such as Schiff base bonds, which provide hydrogels with shear-thinning and self-healing properties, can dynamically break and reform according to external stimuli (e.g., shear) [17–19]. Therefore, the network structure of dynamic covalent bond-based hydrogels can be rearranged under shear via the dynamic bond exchange, which allows liposome microreservoirs to move and spread throughout the hydrogel network [20,21]. As a linear anionic polysaccharide, HA can unite with liposomes to form HA-liposome complexes and collect the mass of liposomes at the interface after structural rearrangements [22]. Thus, incorporating liposomes within the dynamic covalent bond-based HA hydrogels can undergo structural rearrangement in response to shear, and expose internal liposome microreservoirs on the outer surfaces, thus providing stable lubrication. Articular cartilage, covering the ends of the long bones in arthrodial joints, performs as a lubricating, load-bearing surface for smooth articulation [23]. However, cartilage wear is inevitable with aging and even

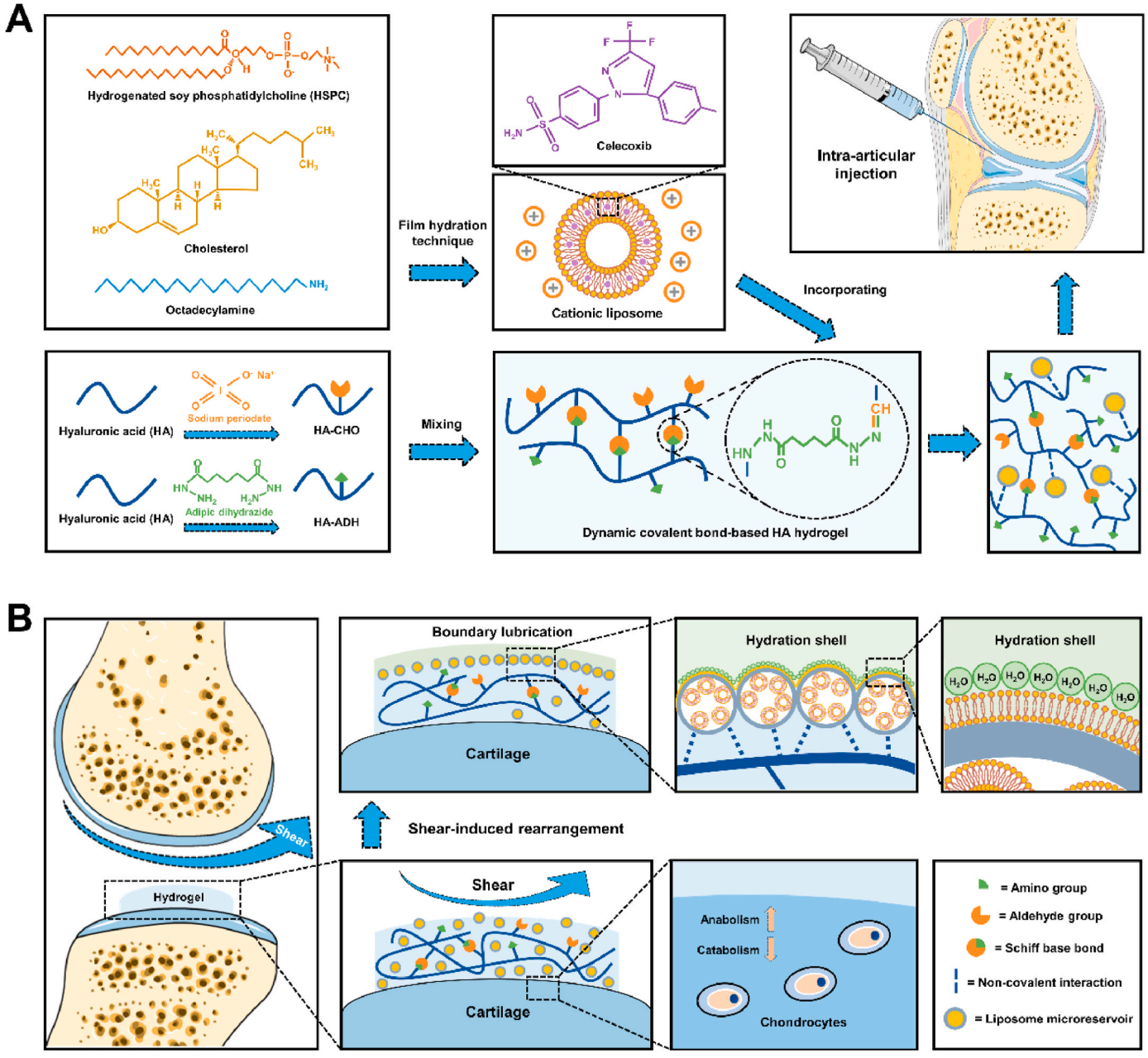

Scheme 1. Schematic illustrations of the fabrication of CLX@Lipo@HA-gel and acting process of repairing osteoarthritic cartilage damage. (A) The CLX@Lipo@HA-gels were constructed by incorporating CLX-loaded HSPC liposomes within Schiff base bond-based HA hydrogels. (B) The CLX@Lipo@HA-gels can expose internal liposome microreservoirs on the outer surfaces to form boundary layers via shear-induced structural rearrangements, and deliver CLX to improve the anabolic-catabolic balance of the ECM.

leads to osteoarthritis if left without proper treatment [24]. Therefore, the intra-articular injection of liposome-containing dynamic covalent bond-based HA hydrogels is supposed to reduce cartilage wear and delay the progression of osteoarthritis via stable boundary lubrication.

As a friction-related joint disease, osteoarthritis can be caused by shear-induced cartilage damage and inflammation [25,26]. This study mixed the aldehyde-modified HA (HA-CHO) and adipic dihydrazide-modified HA (HA-ADH) by Schiff base reaction to obtain dynamic covalent bond-based HA hydrogels. Furthermore, celecoxib (CLX)-loaded HSPC cationic liposomes were integrated into these hydrogels via non-covalent interaction, forming injectable self-healing hydrogels with the function of shear-responsive boundary lubrication and anti-inflammation (Scheme 1A). As presented in Scheme 1B, these hydrogels can expose internal liposome microreservoirs on the outer surfaces under shear via structural rearrangement and form stable boundary layers to reduce friction. In addition, these hydrogels can also relieve joint inflammation and stimulate cartilage matrix formation by delivering anti-inflammatory drugs (i.e., CLX). Based on these advantages, we constructed the shear-responsive boundary-lubricated drug-loaded hydrogels that have tremendous therapeutic potential in treating friction-related diseases like osteoarthritis.

2. Results and discussion

2.1. Preparation and characterization

We chose HA as the backbone macromolecule in this study because HA is the main element in cartilage extracellular matrix (ECM) and has good biocompatibility [27,28]. More importantly, it can combine with liposomes to form liposome reservoirs and restructure under shear to expose liposomes on the sliding surfaces, thus providing stable lubrication [15]. To construct Schiff base bond-based HA hydrogels, HA-CHO and HA-ADH were synthesized to obtain aldehyde groups and amino groups, respectively. ^{1}H NMR spectra confirmed the successful modifications. Two new peaks, corresponding to hemiacetalic protons formed from aldehyde and neighboring hydroxyl groups [29], were detected at 4.9 and 5.0 ppm on the ^{1}H NMR spectrum of HA-CHO. In addition, a new peak (1.5 ppm), which corresponds to methylene proton of conjugated ADH [30], was detected on the ^{1}H NMR spectrum of HA-ADH (Fig. S1).

We chose HSPC lipids to prepare liposomes in this study because HSPC lipids can provide efficient boundary lubrication at physiologically high pressures owing to their robust nature [31,32]. Transmission electron microscope (TEM) analysis of liposomes fabricated by the thin-film hydration technique revealed a spherical appearance of vesicles (Fig. 1A). The mean diameter of the liposomes was 193 nm with a polydispersity index (PDI) of 0.153, indicating good dispersion (Fig. 1B). In addition, the zeta potential of the liposomes was 27.5 ± 4.79 mV (Fig. 1C), which may facilitate the interaction between liposomes and negatively charged HA. To observe the gelation process of the liposome-HA mixtures, HA-CHO (in liposome solutions) and HA-ADH (in liposome solutions) were mixed rapidly and left for gelation. Gelation took place immediately after mixing and was completed in less than 5 min at room temperature (Fig. 1D). To verify that liposomes were successfully incorporated into the hydrogels, laser scanning confocal microscopy (LSCM) was used to observe the Dil-labeled liposomes within the hydrogels. As can be seen from Fig. 1E and F, red fluorescence was distributed within the hydrogels, confirming the successful incorporation of liposomes. Furthermore, we also used a scanning electron microscope (SEM) to observe the surface morphologies of liposome-free HA-based hydrogel (HA-gel) and liposome-incorporating HA-based hydrogel (Lipo@HA-gel). As seen from Fig. 1G and H, a few scattered liposome microreservoirs were observed on the surface of Lipo@HA-gel, while they were absent in HA-gel, indicating that the Lipo@HA-gels can expose liposome microreservoirs on the outer surface to form boundary layers, thus providing a low coefficient of friction (COF).

2.2. Injectability and shear-responsive properties

As presented in Fig. 1I, the Lipo@HA-gels can be easily injected through a syringe with a 0.6 mm needle to draw the letter "LYT" without clogging, indicating that the Lipo@HA-gels can be delivered to closed biological cavities (e.g., joint cavity) by using a minimally invasive puncture needle. Then, we further studied the shear-thinning property of the Lipo@HA-gels using a rheometer. As seen from Fig. 1J, the viscosity of Lipo@HA-gels decreased with increasing shear rates, indicating that the dynamic cross-links in the hydrogel network can be disrupted by shear [33], which may facilitate the migration of liposome microreservoirs.

2.3. Self-healing properties

Since implanted hydrogels can be damaged by external mechanical forces, their self-healing ability is crucial for in vivo applications of hydrogels [34]. The self-healing process was first observed through morphological analysis, in which two separated Lipo@HA-gels healed into one piece without any stimuli after being brought into contact with each other (Fig. S2A). Since the Lipo@HA-gels have free aldehyde and amino groups on the surface, they can form reversible Schiff base bonds after being put together (Fig. S2B). Next, the self-healing property of Lipo@HA-gels was further evaluated by strain sweep and step-strain measurements. The storage modulus (G′) of the Lipo@HA-gels decreased to lower than the loss modulus (G″) at a strain of 480% (Fig. S2C), presenting that the network of Lipo@HA-gels can be disrupted during high strain. In addition, the Lipo@HA-gels exhibited an almost complete recovery of both G′ and G″ once the strain was adjusted to 10%. Furthermore, the disruption-recovery process was reproducible upon additional strain cycles (Fig. S2D), further confirming the excellent self-healing ability of Lipo@HA-gels.

2.4. Shear-responsive boundary lubrication performance

To evaluate the lubrication properties of the shear-responsive boundary-lubricated hydrogels, phosphate buffer saline (PBS), HA-gels, and Lipo@HA-gels were subjected to linear friction tests under the same conditions. As can be seen from Fig. 2A and B, the average COF was significantly higher in the PBS group (0.062 ± 0.007) than in the HA-gel (0.041 ± 0.004, $p < 0.001$) and Lipo@HA-gel (0.031 ± 0.003, $p < 0.001$) groups. Although HA-gel and Lipo@HA-gel groups had similar initial COF, the average COF was significantly lower in the Lipo@HA-gel group than in the HA-gel group ($p < 0.001$). In addition, the wear width analysis showed significantly smaller wear track width in the Lipo@HA-gel group (9.87 ± 1.80 μm) compared to the PBS (27.51 ± 3.62 μm, $p < 0.01$) and HA-gel groups (17.64 ± 3.15 μm, $p < 0.05$) (Fig. 2C and D), which confirmed the outstanding lubrication performance of Lipo@HA-gels.

In further analysis of COF-time plots, we found that the COF values in the HA-gel group decreased in the first 180 s and increased gradually after that (Fig. 2E). Because hydrogels can form fluid films to separate sliding surfaces, the decrease in the COF during the first 180 s is mainly attributed to the fluid film lubrication (blue area) [7]. However, as the friction test went on, the lubricating fluid film cannot be sustained between the opposing surfaces because of the loss of water (Fig. 2F), and the fluid film lubrication can be inactivated, resulting in the increase of COF (red area). As seen from Fig. 2G, similar to HA-gels, the COF values of Lipo@HA-gels decreased during the first 180 s (green area), which is mainly attributed to the fluid film lubrication. However, instead of a continuous increase, we observed a transient increase followed by a sustained decrease of COF values. The transient friction peak is likely because of shear-induced structural rearrangement, which may generate additional energy dissipation [15,22]. During the restructuring, the internal liposome microreservoirs can be exposed on the surface to form stable boundary layers (Fig. 2H). Therefore, the decrease of COF after

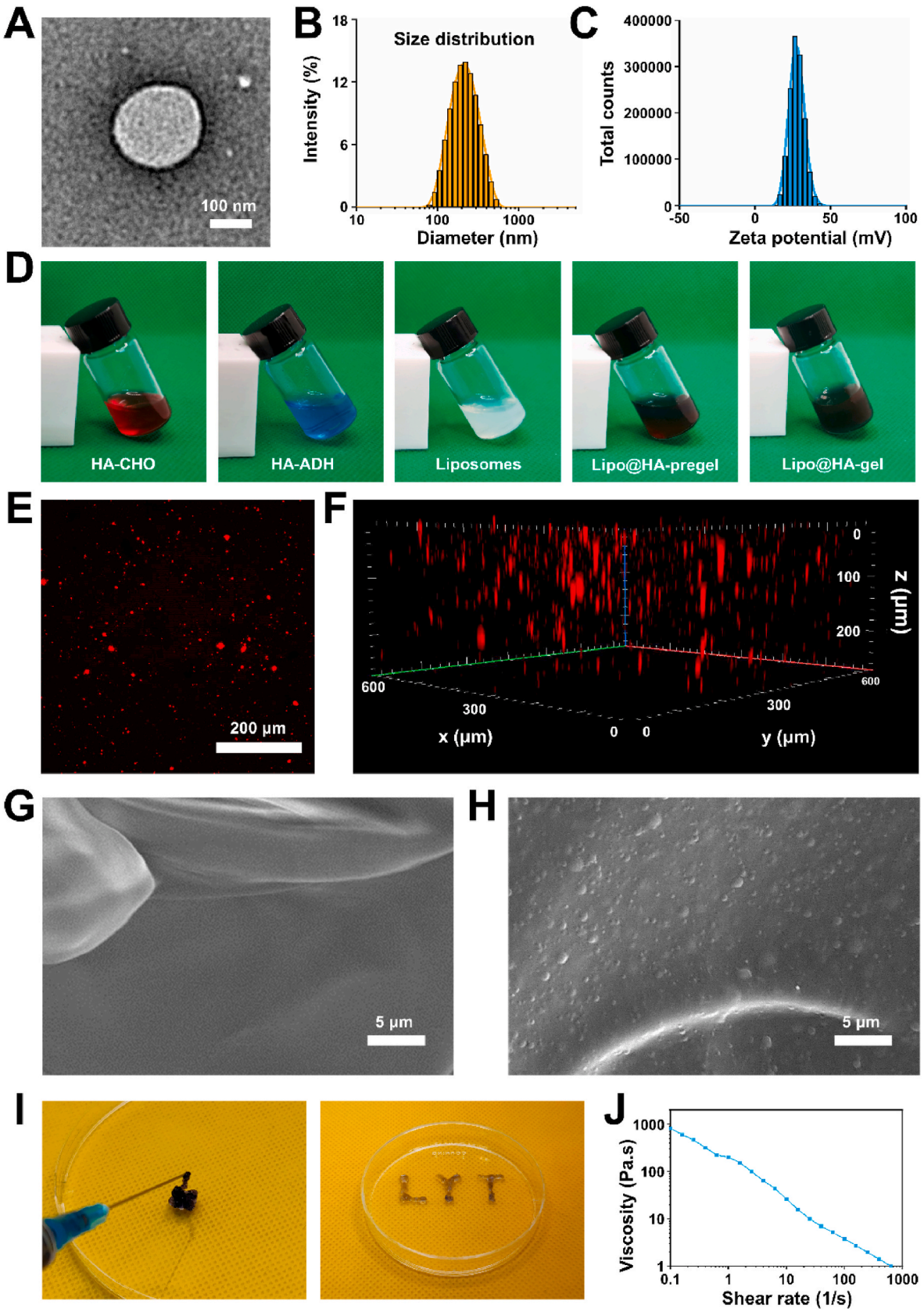

Fig. 1. Characterization of liposomes and Lipo@HA-gels. (A) TEM image of the liposome. (B) Size distribution of liposomes. (C) Zeta potential distribution of liposomes. (D) Solution of HA-CHO, HA-ADH, liposomes, Lipo@HA-pregel, and Lipo@HA-gel. (E) LSCM images of Lipo@HA-gel. (F) Z-stack fluorescent images of Lipo@HA-gel. (G) SEM image of HA-gel. (H) SEM image of Lipo@HA-gel. (I) Photographs of the injectable Lipo@HA-gel, and LYT-type Lipo@HA-gel extruded from a syringe. (J) Viscosity of Lipo@HA-gel at different shear rates.

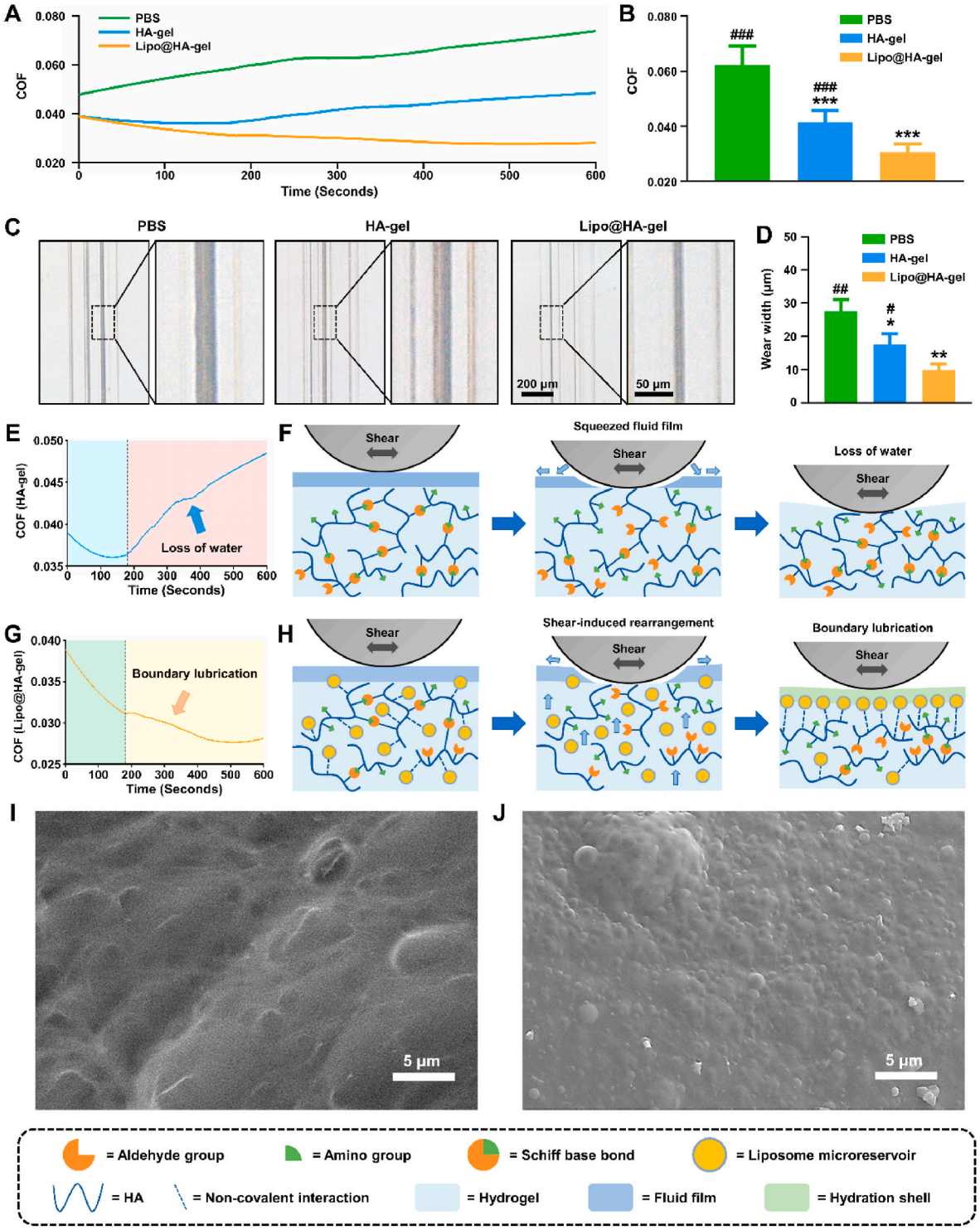

Fig. 2. Lubrication performances of Lipo@HA-gels. (A) COF-time curve for PBS, HA-gels, and Lipo@HA-gels. (B) COF histograms for PBS, HA-gels, and Lipo@HA-gels. (C) Bright-field images of the wear track on the disk tested by PBS, HA-gels, and Lipo@HA-gels. (D) Wear width analysis for the PBS, HA-gel, and Lipo@HA-gel groups. (E) COF-time curve for HA-gels. (F) Schematic showing the lubrication behavior of HA-gels. (G) COF-time curve for Lipo@HA-gels. (H) Schematic showing the lubrication behavior of Lipo@HA-gels. (I) SEM image of the worn HA-gel. (J) SEM image of the worn Lipo@HA-gel. (n = 3, #/##/### and */**/*** indicated $p < 0.05/p < 0.01/p < 0.001$ in comparison with the Lipo@HA-gel and PBS groups, respectively).

the first 180 s is mainly attributed to boundary lubrication (yellow area) [14].

To prove this conjecture, both HA-gels and Lipo@HA-gels that had undergone the abovementioned friction tests (worn HA-gels and worn Lipo@HA-gels) were collected for SEM observation. Similar to newly prepared HA-gels, no liposome microreservoirs were observed on the surface of worn HA-gels (Fig. 2I). Of note, we observed a large number of close-packed liposome microreservoirs on the surface of worn Lipo@HA-gels (Fig. 2J), which seemed to be more than newly prepared Lipo@HA-gels. For further quantification, Dil-labeled liposomes at the surface of the Lipo@HA-gels before and after friction were observed and analyzed under a fluorescence microscope. As seen from Figs. S3A and B,

the worn Lipo@HA-gels (1.52 ± 0.09 fold) had significantly more liposomes on the surface than the newly prepared Lipo@HA-gels (1.00 ± 0.09 fold, $p < 0.01$), indicating that Lipo@HA-gels can restructure under shear and expose internal liposome microreservoirs on the outer surfaces to form boundary layers to provide stable lubrication. In addition, both HA-gels and Lipo@HA-gels recovered their shape gradually after fiction tests, further confirming their self-healing abilities (Fig. S4).

2.5. Degradation properties

The degradation rate is an essential factor that affects the in vivo residence time of lubricating biomaterials [35,36]. However, dynamic covalent hydrogels usually have a relatively fast degradation rate [37], which limits their applications in biolubrication. The degradation experiment exhibited rapid degradation of HA-gels in response to hyaluronidase, and the degradation was almost complete on day 14. In contrast, Lipo@HA-gels exhibited a relatively slow degradation trend and were completely degraded on day 28 (Fig. 3A), possibly because of

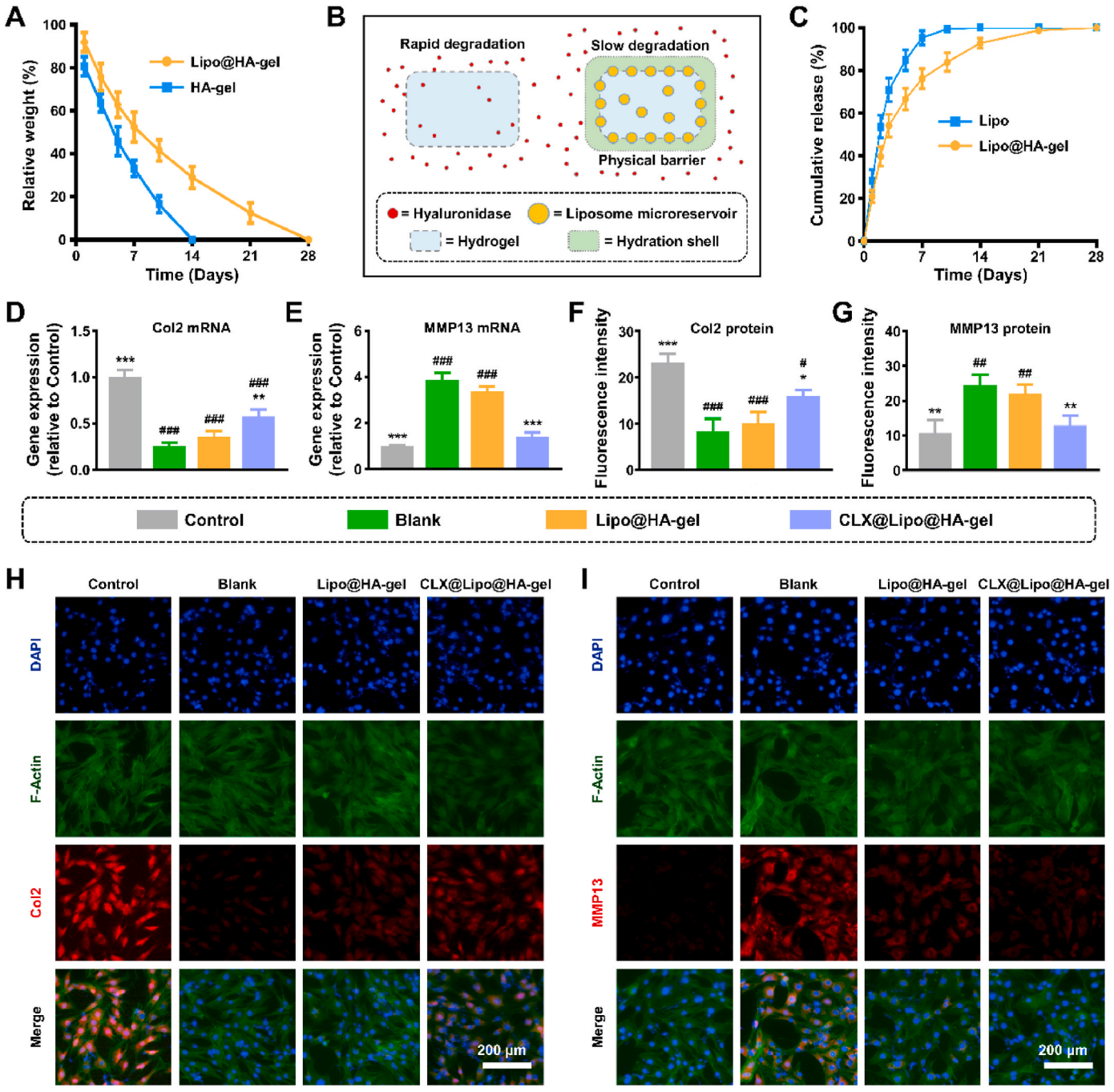

Fig. 3. Degradation, drug loading and release properties of Lipo@HA-gels, and in vitro effects of CLX@Lipo@HA-gels. (A) The degradation curves of HA-gels, and Lipo@HA-gels. (B) Schematic showing the mechanism of retarding the degradation process. (C) Release curves of CLX releasing from liposomes and Lipo@HA-gels. (D) The mRNA expression level of Col2. (E) The mRNA expression level of MMP13. (F) Quantification of Col2 fluorescences. (G) Quantification of MMP13 fluorescences. (H) Representative immunofluorescence images of Col2 protein. (I) Representative immunofluorescence images of MMP13 protein. (n = 3, #/##/### and */**/*** indicated $p < 0.05/p < 0.01/p < 0.001$ in comparison with the control and blank groups, respectively).

the hydration shells surrounding the Lipo@HA-gels, which can act as a physical barrier against enzymatic degradation, thus contributing to sustained lubrication (Fig. 3B) [35,36].

2.6. Drug loading and release properties

CLX, a nonsteroidal anti-inflammatory drug, has been approved to treat osteoarthritis [38]. However, systemic application of CLX is generally associated with the risk of cardiovascular events, while the poor water solubility of CLX limits its topical application [38,39]. Liposome encapsulation can increase the bioavailability of CLX [39], and the drug delivery system can be further stabilized by incorporating liposomes into hydrogels [40,41]. In this study, the encapsulation efficiency of CLX in liposomes and Lipo@HA-gels was 88.57 ± 2.63% and 79.04 ± 2.32%, respectively, indicating that a few drugs leaked out of the liposomes during the mixing process. In addition, the concentration of CLX in liposomes and Lipo@HA-gels were 221.43 ± 6.58 μg/mL and 197.60 ± 5.81 μg/mL, respectively. In the release experiments, liposomes showed a rapid release of 70% of CLX within the first 3 days and a complete release after 10 days. In contrast, Lipo@HA-gels exhibited a relatively slow release of CLX for a period of up to 21 days (Fig. 3C), indicating that hydrogels can stabilize liposomes, thus prolonging the drug release.

2.7. Cell biocompatibility

As an implantable lubricating biomaterial, the CLX-liposome-incorporating HA-based hydrogels (CLX@Lipo@HA-gels) should have good biocompatibility. In this study, the LIVE/DEAD staining and CCK-8 assay were used to evaluate the influences of CLX@Lipo@HA-gels on the viability and proliferation of the C-28/I2 chondrocyte cell line. Almost all cells were alive in 3 days' cultivate without differences between these groups (Figs. S5A and B). In addition, the cell numbers in each group, which were determined by a CCK-8 assay, increased over time without an inter-group difference (Fig. S5C). Overall, the above results indicated that the CLX@Lipo@HA-gels have good biocompatibility and can be applied to biological interfaces to reduce friction.

2.8. Protective effect on cartilage matrix degradation

In addition to abnormal mechanical stress, excessive production of pro-inflammatory cytokines can also cause chondrocyte damage, leading to the biodegradation and synthesis imbalance of ECM [42–44]. Type II collagen (Col2) and aggrecan are the principal constituents of cartilage ECM synthesized by chondrocytes and can be degraded by matrix metalloproteinase 13 (MMP13) and A disintegrin and metallopeptidase with thrombospondin type 1 motif 5 (ADAMTS5) in osteoarthritis conditions [45–48]. In this study, the leaching solution of the anti-inflammatory drug (CLX)-loaded hydrogels was cultured with pro-inflammatory cytokine-stimulated chondrocytes (C-28/I2), and the expressions of Col2, aggrecan, MMP13, and ADAMTS5 were used to evaluate the levels of anabolic and catabolic activities.

The RT-qPCR results indicated that the expressions of anabolic genes (Col2 and aggrecan) were significantly higher in the CLX@Lipo@HA-gel group (0.58 ± 0.07 fold; 0.74 ± 0.03 fold) than in the blank group (0.26 ± 0.04 fold, $p < 0.01$; 0.41 ± 0.04 fold, $p < 0.001$). In addition, the expressions of catabolic genes (MMP13 and ADAMTS5) were significantly lower in the CLX@Lipo@HA-gel (1.42 ± 0.19 fold; 1.67 ± 0.09 fold) group than in the blank group (3.88 ± 0.31 fold, $p < 0.001$; 3.10 ± 0.41 fold, $p < 0.01$) (Fig. 3D and E, Figs. S6A and B). Similarly, the protein expressions of Col2 and MMP13 were significantly higher and lower, respectively, in the CLX@Lipo@HA-gel group (15.91 ± 1.25; 12.93 ± 2.74) than in the blank group (8.28 ± 2.75, $p < 0.05$; 24.60 ± 2.85, $p < 0.01$) (Fig. 3F–I). These outcomes indicated that the CLX@Lipo@HA-gels could promote anabolism and suppress catabolic processes by delivering CLX.

2.9. Therapeutic effect on osteoarthritis in vivo

In this study, destructive surgical models of osteoarthritis in rats were established to alter the mechanical stability of knee joints and induce cartilage damage [49]. On the X-ray plain, osteoarthritic cartilage damage is often characterized by joint space narrowing [50,51]. As presented in Fig. 4A–C, PBS (0.68 ± 0.05 fold, $p < 0.01$; 0.26 ± 0.12 fold, $p < 0.01$), HA-gel (0.77 ± 0.08 fold, $p < 0.05$; 0.35 ± 0.14 fold, $p < 0.01$), and Lipo@HA-gel (0.80 ± 0.07 fold, $p < 0.05$; 0.46 ± 0.14 fold, $p < 0.01$) groups have significantly narrower joint space widths (JSWs), which were obtained from the anterior-posterior (AP) and lateral (LAT) views, than the sham group (1.00 ± 0.07 fold; 1.00 ± 0.17 fold), without an inter-group difference. In contrast, the JSWs (obtained from the AP and LAT views) in the CLX@Lipo@HA-gel group (0.89 ± 0.07 fold, $p < 0.05$; 0.87 ± 0.17 fold, $p < 0.01$) were broader than in the PBS group, yet there was no significant difference when compared with the sham group. In addition to JSW, we also used Kellgren-Lawrence (KL) scores to grade the osteoarthritis. As seen from Fig. S7, the modified KL scores were significantly lower in the CLX@Lipo@HA-gel group (1.20 ± 0.45) than in the PBS group (2.40 ± 0.55, $p < 0.01$). Osteophyte formation is considered as a compensation for joint damage and is another pathogenic characteristic of osteoarthritis [52,53]. In this study, no apparent osteophyte formation was observed in the sham group, but it was present in the osteoarthritis groups. However, after intra-articular injection of CLX@Lipo@HA-gels, the osteophyte volume was markedly reduced in the CLX@Lipo@HA-gel group (1.00 ± 0.08 fold) when compared to the PBS group (1.34 ± 0.05 fold, $p < 0.01$) (Fig. 4D and E).

Except as imaging examination, histological analysis on articular cartilage was conducted by hematoxylin and eosin (H&E), toluidine blue, and Safranin O-fast green staining. As illustrated in Fig. 5A, the sham group has a smooth and continuous cartilage surface, clear structure, normal cellularity, and uniformly stained cartilage ECM. The PBS group revealed cartilage erosion, disorganized structure, apparent cellular abnormalities, and weak staining. In contrast, these degenerative changes were significantly ameliorated in the CLX@Lipo@HA-gel group, supported by Mankin scores (Fig. 5B). Notably, although the Lipo@HA-gel group exhibited similar cellular and staining results to PBS controls, the articular cartilage in the Lipo@HA-gel group has a better structure and smoother surface than the PBS group, and showed no significant difference compared with the CLX@Lipo@HA-gel and sham groups, indicating that the Lipo@HA-gel can function as a bio lubricant at joint interfaces.

Furthermore, we also analyzed Col2 and MMP13 protein expressions by immunohistochemistry. The sham (0.98 ± 0.11 fold, $p < 0.001$; 1.00 ± 0.11 fold, $p < 0.01$) and CLX@Lipo@HA-gel (0.85 ± 0.13 fold, $p < 0.001$; 1.09 ± 0.26 fold, $p < 0.01$) groups have significantly higher Col2 expression protein levels and lowered MMP13 expression protein levels than the PBS group (0.42 ± 0.09 fold; 2.62 ± 0.47 fold) (Fig. 6). Moreover, the level of MMP13 protein expression in the Lipo@HA-gel group (1.98 ± 0.21 fold) was significantly lower than the PBS group ($p < 0.05$), although it remained higher than that of the sham ($p < 0.001$) and CLX@Lipo@HA-gel ($p < 0.01$) groups. The reason for this may be that the Lipo@HA-gels can act as a bio lubricant to reduce frictional wear and chondrocyte damage, thus decreasing the production of MMP13. In sum, these results demonstrated that CLX@Lipo@HA-gels could act both as biolubricants and drug-delivery vehicles to alleviate cartilage wear, reduce osteophyte formation, promote cartilage ECM formation and inhibit cartilage degradation, thus attenuating the osteoarthritis progression.

2.10. Limitations

This study has several limitations. First, this study only provided a rough evaluation of the enzymatic degradation properties of the hydrogels by measuring their residual weight. Further study (e.g., HA molecular weight analysis) is still needed. Second, the polyethylene (PE)

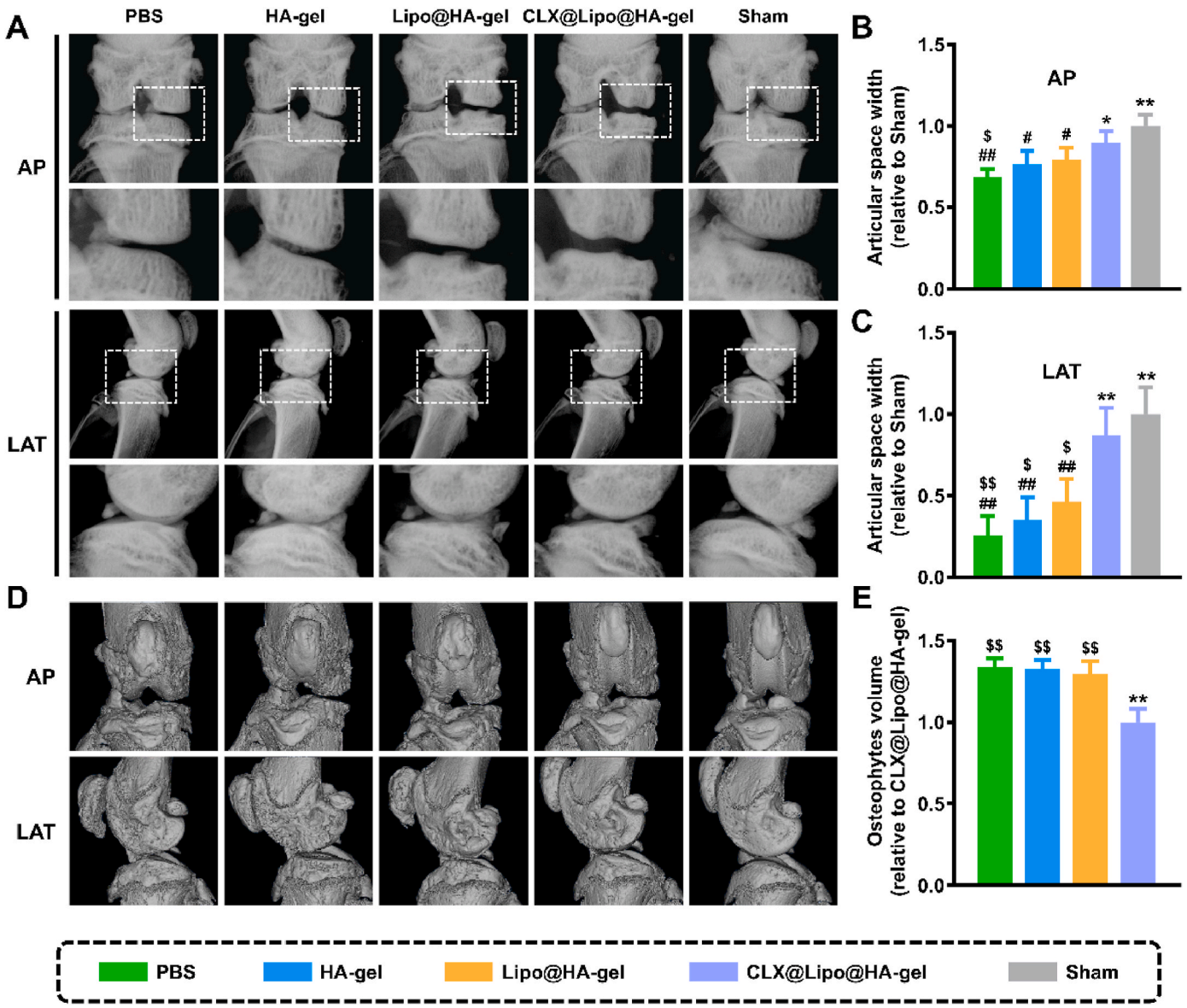

Fig. 4. Radiographic evaluation. (A) Representative X-ray images in AP and LAT view of the knee joint. (B) The relative JSW measured from AP images. (C) The relative JSW measured from LAT images. (D) Representative MicroCT images in AP and LAT view of the knee joint. (E) The relative osteophyte volume measured from MicroCT images. (#/##, $/$$ and */** indicated $p < 0.05/p < 0.01$ compared to the sham, CLX@Lipo@HA-gel and PBS groups, respectively).

sphere and stainless-steel disk rather than physiological surfaces (e.g., cartilage) were used as counter-faces for in vitro friction tests. However, whether the gliding is PE on steel or cartilage on cartilage, the basic strategies are similar. In addition, the friction tests were performed under physiological joint pressure (25 MPa). Therefore, results obtained on the PE/steel friction may also be of relevance for cartilage lubrication. Third, only small animals (rats) were used for in vivo evaluation. Since small and large animals have different anatomical structures and body shapes [54], further exploration of this material using large animal experiments is needed.

3. Conclusion

In this study, we have developed an injectable shear-responsive boundary-lubricated drug-loaded hydrogel by incorporating CLX-loaded HSPC liposomes within dynamic covalent bond-based HA hydrogels. The CLX@Lipo@HA-gels can restructure in response to shear and expose internal liposome microreservoirs on the outer surfaces to form lipid-based boundary layers, providing stable lubrication. Furthermore, instead of acting as a pure boundary biolubricant, CLX@Lipo@HA-gel can also serve as a drug delivery vehicle to alleviate inflammation-induced ECM degradation by delivering CLX. In general, we anticipate that such a liposome-incorporating dynamic covalent bond-based HA hydrogel would open new avenues for treating friction-related diseases like osteoarthritis.

4. Experimental procedures

4.1. Synthesis of HA-CHO

In brief, 0.8 g of HA (molecular weight = 800–1500 kDa; Macklin, China) was dissolved in deionized water (90 mL), and this reacted with 450 mg sodium periodate (Sangon, China) for 4 h. Afterward, ethylene glycol (500 μL) was used to terminate the reaction. The product was then purified using the dialysis method and lyophilized. The successful oxidization of HA was validated by ^{1}H NMR (600 MHz, Bruker, Germany).

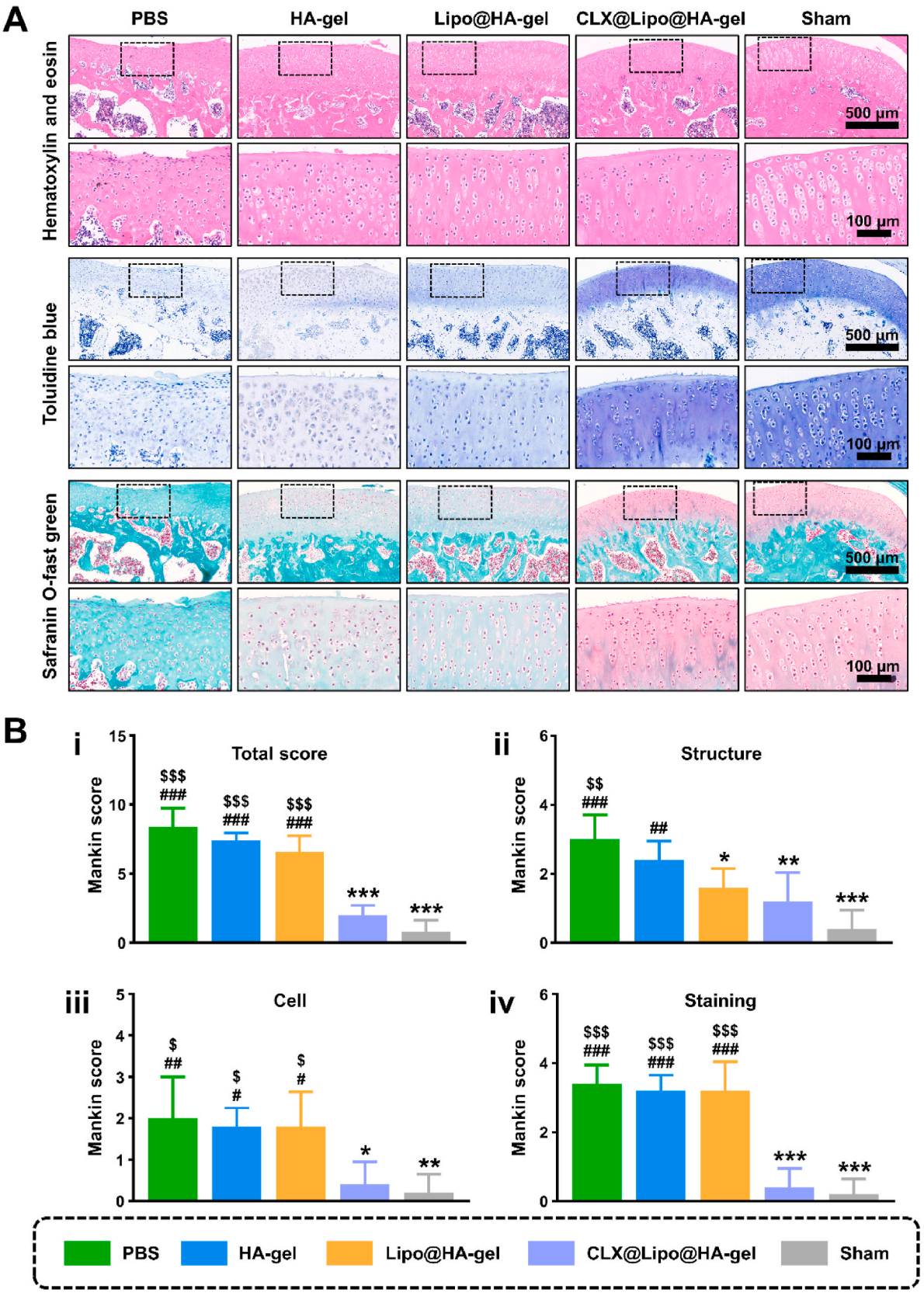

Fig. 5. Histological staining. (A) Representative images of H&E staining, Toluidine Blue staining, and Safranin O-fast green staining from each group. (B) The modified Mankin scores: i) total Mankin scores, and Mankin Score presented as ii) cartilage structure, iii) cellular abnormalities, and iv) matrix staining. (#/##/###, $/$$/$$$ and */**/*** indicated $p < 0.05/p < 0.01/p < 0.001$ compared to the sham, CLX@Lipo@HA-gel and PBS groups, respectively).

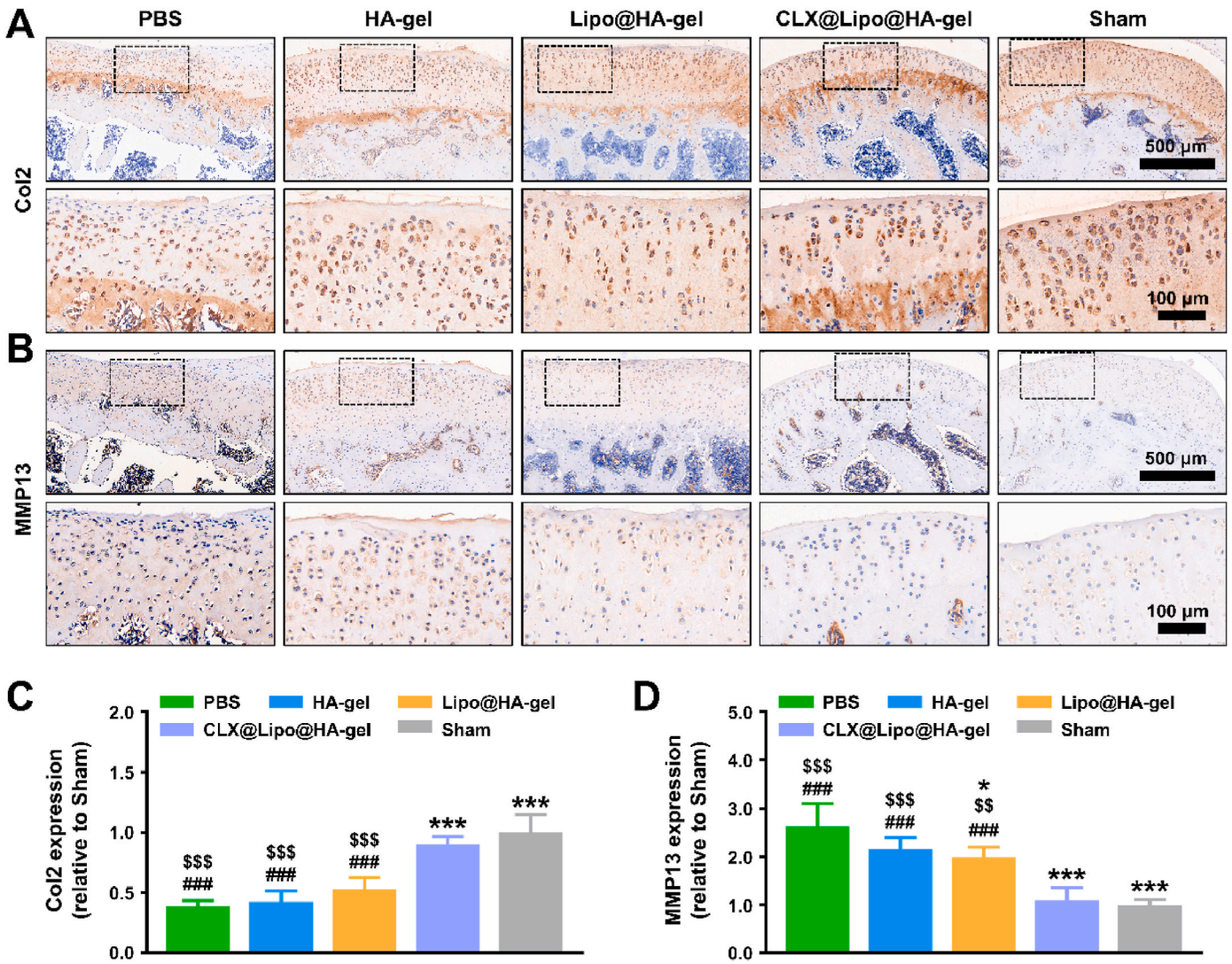

Fig. 6. Immunohistochemistry staining. (A) Representative images of Col2 protein immunohistochemical staining. (B) Representative images of MMP13 protein immunohistochemical staining. (C) Quantification of relative Col2 expression. (D) Quantification of relative MMP13 expression. (#/###/###, $/$$/$$$ and */**/*** indicated $p < 0.05/p < 0.01/p < 0.001$ compared to the sham, CLX@Lipo@HA-gel and PBS groups, respectively).

4.2. Synthesis of HA-ADH

Briefly, 2 g of HA (molecular weight = 800–1500 kDa; Macklin, China) was dissolved in deionized water (100 mL), to which 4.58 g ADH (Macklin, China) was added. Afterward, 2.02 g of 1-ethyl-3-(3-dimethylaminopropyl) carbodiimide hydrochloride (EDC, Macklin, China) and 1.42 g of 1-Hydroxybenzotriazole (HOBt, Macklin, China) were added dropwise. The pH of the solution was regulated to 6.8 by HCL (2 M) and the reaction took place all night. The product was then purified using the dialysis method and lyophilized. ^{1}H NMR confirmed the successful synthesis of HA-ADH.

4.3. Fabrication and characterization of cationic liposomes

In brief, 20 mg HSPC (A.V.T. Pharmaceutical Co. Ltd., China), 5 mg cholesterol (Sangon, China), 2 mg octadecylamine (Aladdin, China), and 1 mg CLX (Macklin, China) were dissolved into 5 mL chloroform. The mixed solution was then evaporated at 60 °C to obtain dried lipid film. Subsequently, 4 mL deionized water was added, followed by a 20-minute sonication. Afterward, the liposome solution was extruded through 0.45- and 0.22-μm membrane filters (Millex, Ireland). The morphologies of the liposomes were observed by TEM (FEI Talos L120C, USA). The size, PDI, and zeta potential of the liposomes were analyzed by the dynamic light scattering method using a Zetasizer (Malvern Nano-ZS, UK).

4.4. Preparation and characterization of hydrogels

For the preparation of the Lipo@HA-gel, HA-CHO and HA-ADH were dissolved in the abovementioned liposome solution at 25 mg/mL, respectively, and were mixed at a ratio of 3:1 (vol/vol). For the preparation of the HA-gel, liposomes were absent in the reaction mixture. The gelation was observed visually when kept at indoor temperature. The surface morphologies of Lipo@HA-gel and HA-gel were observed using a SEM (FEI Sirion 200, USA). The Dil (Beyotime, China) -labeled liposomes were used to confirm the successful incorporation of liposomes and were observed using an LSCM (ZEISS, Germany).

4.5. Shear-thinning evaluation

The injectability of the Lipo@HA-gel was evaluated using a disposable syringe (inner aperture diameter of 0.6 mm) that extruded the Lipo@HA-gel through the syringe using hand pressure at room temperature. In addition, the relationships of shear rate with viscosity were explored to evaluate the shear-thinning properties of the Lipo@HA-gel

using a Discovery hybrid rheometer-2 (HR-2, USA) with a 40 mm steel Peltier plate.

4.6. Self-healing evaluation

The self-healing behavior of the Lipo@HA-gel was evaluated using macroscopic and rheological methods. For the macroscopic evaluation, two pieces of the Lipo@HA-gels were dyed with different colors (red and blue) and kept in contact with each other, and the self-healing process was observed visually. In addition, the rheological analysis was used to evaluate the self-healing capacity of the Lipo@HA-gel. In brief, a strain amplitude sweep test was performed with a strain amplitude ranging from 0.01 to 1500% to obtain the critical strain point. Afterward, an alternate step strain sweep test was performed at a constant frequency of 10 rad/s. The oscillatory strain was switched between 10% and 800%, ensuring a duration of 60 s for each strain value.

4.7. Tribological test

The lubrication performances of the PBS, HA-gel, and Lipo@HA-gel were evaluated and compared using a universal materials tester (UMT-3, Bruker, Germany) in a linear reciprocating mode. Stainless steel disk (Poisson's ratio: 0.3; elastic modulus: 194 GPa) was used as the bottom surface, and a PE sphere (diameter: 8 mm; Poisson's ratio: 0.4; elastic modulus: 1 GPa) was used as the top surface. The oscillation amplitude, frequencies, applied load, and test time were 4 mm, 1 Hz, 1 N, and 600 s, respectively. The COF measurements started 0.495 s after the oscillation was started, and the data were recorded at 1-s intervals. According to the Hertz equation, the applied load (1 N) corresponds to a maximum contact pressure of 25.68 MPa [55], which is similar to the physiological pressure of joints [15]. After the experiment, the wear tracks formed on the surface of the stainless-steel disk were observed under a bright-field microscope and were used for wear width analysis. In addition, the HA-gel and Lipo@HA-gel were collected and observed macroscopically and under SEM. Furthermore, the liposomes at the surface of the Lipo@HA-gels before and after friction were labeled by Dil dye and then observed under a fluorescence microscope.

4.8. Degradation tests

The degradation tests of HA-gel/Lipo@HA-gel were conducted in 1 mL PBS (pH = 7.4) containing 5 mg hyaluronidase (Beijing Labgic Technology Co., Ltd., China) at 37 °C. The remaining sample was weighed at every time point, and the results were compared to their initial weight.

4.9. Drug encapsulation and release

The encapsulation efficiency of the CLX was measured using a UV-5100 UV–visible spectrophotometer (Metash, China), and the release profile of the CLX was carried out using the dialysis membrane method. In brief, Lipo@HA-gels/liposomes were firstly transferred to a dialysis bag. The dialysis bag was then immersed in 10 mL of PBS (pH = 7.4) and oscillated in a shaker incubator at 37 °C until the maximum drug release was achieved. The release medium (1 mL) was collected for UV analysis and replaced with an isopyknic PBS at scheduled time intervals.

4.10. Biocompatibility test

C-28/I2 (Otwo Biotech, Inc., China, Catalogue No. HTX2308), a human immortalized chondrocyte cell line [56], was used throughout this study. The biocompatibility of hydrogels was evaluated by employing a direct contact between hydrogels and C-28/I2 cells. Briefly, after the C-28/I2 cells were attached to the wells, the hydrogels were added. After co-culture for 1, 2, and 3 days, the hydrogels were gently removed from the wells, and the wells were washed by PBS twice to remove any residual hydrogel. Afterward, a LIVE/DEAD staining assay (Beyotime, China) was used to discriminate live cells from dead cells, and a cell counting kit-8 (CCK-8) assay (Beyotime, China) was used to access cell proliferation. C-28/I2 cells cultured without hydrogels served as control. All steps were performed according to manufacturing guidelines.

4.11. Osteoarthritis cell model

To evaluate the anti-inflammatory effects of hydrogels, Lipo@HA-gels/CLX@Lipo@HA-gels were immersed in a culture medium for 2 weeks, and the supernatants (leaching solution) were collected for subsequent cell experiments. Pro-inflammatory cytokine interleukin (IL)-1β is widely used to induce an osteoarthritis-like inflammatory response [57,58], which can induce the production of MMPs, and reduce the synthesis of Col2 [59]. In this study, C-28/I2 cells were exposed to 10 ng/mL IL-1β (PeproTech, China), and cultured with normal culture medium, or the above leaching solution. C-28/I2 cells treated without IL-1β served as control.

4.12. Detection of mRNA expression

Total RNA was isolated from C-28/I2 cells via RNA extraction solution (Servicebio, China) and transcribed to cDNA using RevertAid First Strand cDNA Synthesis Kit (Thermo, USA). Subsequently, the ABI 7300 real-time PCR system (ABI, USA) was used to perform RT-PCR. Primer sequences (Col2, aggrecan, MMP13, ADAMTS5, and GADPH) are listed in Table S1. The comparative CT (ΔΔCT) method was used to quantify the relative mRNA expression.

4.13. Immunofluorescence staining

After fixation in 4% paraformaldehyde (Servicebio, China) for 15 min, C-28/I2 cells were incubated with rabbit anti-Col2/MMP13 primary antibody (Servicebio, China) at 4 °C overnight, followed by incubating with Cy3-conjugated goat anti-rabbit IgG (Servicebio, China) for 50 min. Afterward, fluorescein isothiocyanate -conjugated phalloidin and DAPI (Servicebio, China) were used to stain the actin cytoskeleton and nuclei, respectively. The samples were observed using an LSCM.

4.14. Osteoarthritis rat model

All animal work performed was authorized by the Research Ethics Committee of the First Affiliated Hospital of Chongqing Medical University (2021-207). Osteoarthritis models were established by anterior cruciate ligament transection and medial meniscus resection (ACLT + MMx) using Sprague Dawley rats (male, 12 weeks old).

Cartilage-adhesive hydrogels, which can simultaneously adhere to the upper and lower articular surfaces, will prevent the relative motion between the articular surfaces, thereby decreasing their ability to lubricate. In addition, the joint cavity is a closed space, and the injected hydrogels are confined between the upper and lower articular surfaces. Therefore, by adjusting the injection volume, the hydrogels can function in vivo without adhesion ability. It is reported that 30 μL of the solution can fill up the cavity of the rat knee's joint without overflowing [60]. Thus, an injection volume of 30 μL was chosen in this study.

After modeling, the osteoarthritis rats were randomized into 4 groups (5 rats per group), and received 30 μL intraarticular injections of PBS, HA-gels, Lipo@HA-gels, and CLX@Lipo@HA-gels (containing 5.93 ± 0.17 μg CLX), respectively, at the 1st and 4th week. Rats in the sham group (n = 5) received anesthesia and skin incision only. All rats were sacrificed at the 8th week.

4.15. Radiographic evaluation

After 8 weeks of modeling, X-ray radiography was performed using a

Faxitron X-ray machine (Faxitron X-ray, USA) with 10-s exposure under 32 kV. The X-ray images were taken from the AP and LAT orientations to measure the JSW. The degree of radiological osteoarthritis was assessed by two blinded observers according to the modified KL scoring system [61]. For further evaluation, the knee samples were harvested and analyzed by using a microCT system (SkyScan 1172, Belgium).

4.16. Histologic and immunohistochemical examinations

After 8 weeks of modeling, the harvested knee joints were fixed, decalcified, embedded, and sagittally sectioned (5 μm). H&E, toluidine blue, and Safranin O-fast green were used to stain the sections for histologic analysis. Pathology scores (the modified Mankin scores) were evaluated for each section by two blinded observers [62]. For immunohistochemical staining, rabbit polyclonal anti-Col2/MMP13 (Servicebio, China) antibodies were used to incubate the sections overnight at 4 °C. After incubating with goat anti-rabbit secondary antibodies for 1 h, the sections were allowed to react with DAB reagents. Appropriate negative controls without primary antibodies were included in immunohistochemistry protocols to confirm specificity. The relative expressions of Col2 and MMP13 were quantified using the Image J 1.46r software (Wayne Rasband, NIH, USA).

4.17. Statistical analysis

All in vitro experiments were conducted in triplicate, and all data were presented as mean ± standard deviation. We used one-way ANOVA and Tukey's post hoc test to analyze data via SPSS 26.0 software (SPSS Inc., USA). $p < 0.05$ denoted the statistical significance.

CRediT authorship contribution statement

Yiting Lei: Conceptualization, Methodology, Investigation, Data curation, Writing – original draft, preparation. **Xingkuan Wang:** Methodology, Investigation, Data curation, Writing – original draft, preparation. **Junyi Liao:** Methodology, Investigation, Data curation, Writing – original draft, preparation. **Jieliang Shen:** Methodology, Investigation, Data curation. **Yuling Li:** Methodology, Investigation, Data curation. **Zhengwei Cai:** Methodology, Investigation, Data curation. **Ning Hu:** Conceptualization, Supervision, Resources. **Xiaoji Luo:** Supervision, Resources, Funding acquisition. **Wenguo Cui:** Conceptualization, Visualization, Supervision, Resources, Funding acquisition, Project administration, Writing – review & editing. **Wei Huang:** Conceptualization, Supervision, Resources, Funding acquisition, Project administration.

Declaration of competing interest

The authors declare that they have no known competing financial interests or personal relationships that could have appeared to influence the work reported in this paper.

Acknowledgements

This work was supported by the National Key Research and Development Program of China (2020YFA0908200), the National Natural Science Foundation of China (81873998, 32101104 and 81972069), and Shanghai Jiao Tong University "Medical and Research" Program (ZH2018ZDA04).

Appendix A. Supplementary data

Supplementary data to this article can be found online at https://doi.org/10.1016/j.bioactmat.2022.02.016.

References

[1] B.G. Cooper, B. Catalina, A. Nazarian, B.D. Snyder, M.W. Grinstaff, Active agents, biomaterials, and technologies to improve biolubrication and strengthen soft tissues, Biomaterials 181 (2018) 210–226.
[2] E. Liamas, S.D. Connell, M. Zembyla, R. Ettelaie, A. Sarkar, Friction between soft contacts at nanoscale on uncoated and protein-coated surfaces, Nanoscale 13 (4) (2021) 2350–2367.
[3] Y. Piao, H. You, T. Xu, H.-P. Bei, I.Z. Piwko, Y.Y. Kwan, X. Zhao, Biomedical applications of gelatin methacryloyl hydrogels, Eng. Regen. 2 (2021) 47–56.
[4] J. Ouyang, X. Ji, X. Zhang, C. Feng, Z. Tang, N. Kong, A. Xie, J. Wang, X. Sui, L. Deng, Y. Liu, J.S. Kim, Y. Cao, W. Tao, In situ sprayed NIR-responsive, analgesic black phosphorus-based gel for diabetic ulcer treatment, Proc. Natl. Acad. Sci. U. S. A. 117 (46) (2020) 28667–28677.
[5] T.A. Schmidt, Lubricating lipids in hydrogels, Science 370 (6514) (2020) 288–289.
[6] D. Xu, J. Huang, D. Zhao, B. Ding, L. Zhang, J. Cai, High-flexibility, high-toughness double-cross-linked chitin hydrogels by sequential chemical and physical cross-linkings, Adv. Mater. 28 (28) (2016) 5844–5849.
[7] W. Lin, J. Klein, Recent progress in cartilage lubrication, Adv. Mater. 33 (18) (2021), e2005513.
[8] L. Ma, A. Gaisinskaya-Kipnis, N. Kampf, J. Klein, Origins of hydration lubrication, Nat. Commun. 6 (2015) 6060.
[9] J. Li, W. Cao, Z. Wang, M. Ma, J. Luo, Origin of hydration lubrication of zwitterions on graphene, Nanoscale 10 (35) (2018) 16887–16894.
[10] E.D. Bonnevie, D. Galesso, C. Secchieri, I. Cohen, L.J. Bonassar, Elastoviscous transitions of articular cartilage reveal a mechanism of synergy between lubricin and hyaluronic acid, PLoS One 10 (11) (2015), e0143415.
[11] T.A. Schmidt, N.S. Gastelum, Q.T. Nguyen, B.L. Schumacher, R.L. Sah, Boundary lubrication of articular cartilage: role of synovial fluid constituents, Arthritis Rheum. 56 (3) (2007) 882–891.
[12] T.E. Ludwig, M.M. Hunter, T.A. Schmidt, Cartilage boundary lubrication synergism is mediated by hyaluronan concentration and PRG4 concentration and structure, BMC Muscoskel. Disord. 16 (2015) 386.
[13] S. Jahn, J. Klein, Hydration lubrication: the macromolecular domain, Macromolecules 48 (15) (2015) 5059–5075.
[14] W. Lin, M. Kluzek, N. Iuster, E. Shimoni, N. Kampf, R. Goldberg, J. Klein, Cartilage-inspired, lipid-based boundary-lubricated hydrogels, Science 370 (6514) (2020) 335–338.
[15] A. Dėdinaitė, D.C.F. Wieland, P. Bełdowski, P.M. Claesson, Biolubrication synergy: hyaluronan - Phospholipid interactions at interfaces, Adv. Colloid Interface Sci. 274 (2019) 102050.
[16] R. Sorkin, Y. Dror, N. Kampf, J. Klein, Mechanical stability and lubrication by phosphatidylcholine boundary layers in the vesicular and in the extended lamellar phases, Langmuir 30 (17) (2014) 5005–5014.
[17] Z. Tang, Q. Huang, Y. Liu, Y. Chen, B. Guo, L. Zhang, Uniaxial stretching-induced alignment of carbon nanotubes in cross-linked elastomer enabled by dynamic cross-link reshuffling, ACS Macro Lett. 8 (12) (2019) 1575–1581.
[18] Y. Tu, N. Chen, C. Li, H. Liu, R. Zhu, S. Chen, Q. Xiao, J. Liu, S. Ramakrishna, L. He, Advances in injectable self-healing biomedical hydrogels, Acta Biomater. 90 (2019) 1–20.
[19] N. Zheng, Y. Xu, Q. Zhao, T. Xie, Dynamic covalent polymer networks: a molecular platform for designing functions beyond chemical recycling and self-healing, Chem. Rev. 121 (3) (2021) 1716–1745.
[20] N. Lopez Mora, M. Owens, S. Schmidt, A.F. Silva, M. Bradley, Poly-epsilon-lysine hydrogels with dynamic crosslinking facilitates cell proliferation, Materials 13 (17) (2020).
[21] W. Zou, J. Dong, Y. Luo, Q. Zhao, T. Xie, Dynamic covalent polymer networks: from old chemistry to modern day innovations, Adv. Mater. 29 (14) (2017).
[22] A. Raj, M. Wang, T. Zander, D.C.F. Wieland, X. Liu, J. An, V.M. Garamus, R. Willumeit-Römer, M. Fielden, P.M. Claesson, A. Dėdinaitė, Lubrication synergy: mixture of hyaluronan and dipalmitoylphosphatidylcholine (DPPC) vesicles, J. Colloid Interface Sci. 488 (2017) 225–233.
[23] G.A. Orozco, P. Tanska, C. Florea, A.J. Grodzinsky, R.K. Korhonen, A novel mechanobiological model can predict how physiologically relevant dynamic loading causes proteoglycan loss in mechanically injured articular cartilage, Sci. Rep. 8 (1) (2018) 15599.
[24] E.A. Aisenbrey, G. Bilousova, K. Payne, S.J. Bryant, Dynamic mechanical loading and growth factors influence chondrogenesis of induced pluripotent mesenchymal progenitor cells in a cartilage-mimetic hydrogel, Biomater Sci 7 (12) (2019) 5388–5403.
[25] X. Ji, Y. Yan, T. Sun, Q. Zhang, Y. Wang, M. Zhang, H. Zhang, X. Zhao, Glucosamine sulphate-loaded distearoyl phosphocholine liposomes for osteoarthritis treatment: combination of sustained drug release and improved lubrication, Biomater Sci 7 (7) (2019) 2716–2728.
[26] R.L. Trevino, C.A. Pacione, A.M. Malfait, S. Chubinskaya, M.A. Wimmer, Development of a cartilage shear-damage model to investigate the impact of surface injury on chondrocytes and extracellular matrix wear, Cartilage 8 (4) (2017) 444–455.
[27] Y. Wang, W. Zhang, P. Sun, Y. Cai, W. Xu, Q. Fan, Q. Hu, W. Han, A novel multimodal NIR-II nanoprobe for the detection of metastatic lymph nodes and targeting chemo-photothermal therapy in oral squamous cell carcinoma, Theranostics 9 (2) (2019) 391–404.
[28] M. Dovedytis, Z.J. Liu, S. Bartlett, Hyaluronic acid and its biomedical applications: a review, Eng. Regen. 1 (2020) 102–113.
[29] L. Li, N. Wang, X. Jin, R. Deng, S. Nie, L. Sun, Q. Wu, Y. Wei, C. Gong, Biodegradable and injectable in situ cross-linking chitosan-hyaluronic acid based

hydrogels for postoperative adhesion prevention, Biomaterials 35 (12) (2014) 3903–3917.
[30] Y. Amano, S. Ohta, K.L. Sakura, T. Ito, Pemetrexed-conjugated hyaluronan for the treatment of malignant pleural mesothelioma, Eur. J. Pharmaceut. Sci. 138 (2019) 105008.
[31] L. Zhu, J. Seror, A.J. Day, N. Kampf, J. Klein, Ultra-low friction between boundary layers of hyaluronan-phosphatidylcholine complexes, Acta Biomater. 59 (2017) 283–292.
[32] J. Yu, X. Banquy, G.W. Greene, D.D. Lowrey, J.N. Israelachvili, The boundary lubrication of chemically grafted and cross-linked hyaluronic acid in phosphate buffered saline and lipid solutions measured by the surface forces apparatus, Langmuir 28 (4) (2012) 2244–2250.
[33] V. Yesilyurt, M.J. Webber, E.A. Appel, C. Godwin, R. Langer, D.G. Anderson, Injectable self-healing glucose-responsive hydrogels with pH-regulated mechanical properties, Adv. Mater. 28 (1) (2016) 86–91.
[34] L. Li, B. Yan, J. Yang, L. Chen, H. Zeng, Novel mussel-inspired injectable self-healing hydrogel with anti-biofouling property, Adv. Mater. 27 (7) (2015) 1294–1299.
[35] Y. Han, J. Yang, W. Zhao, H. Wang, Y. Sun, Y. Chen, J. Luo, L. Deng, X. Xu, W. Cui, H. Zhang, Biomimetic injectable hydrogel microspheres with enhanced lubrication and controllable drug release for the treatment of osteoarthritis, Bioact Mater 6 (10) (2021) 3596–3607.
[36] J. Yang, Y. Han, J. Lin, Y. Zhu, F. Wang, L. Deng, H. Zhang, X. Xu, W. Cui, Ball-bearing-Inspired polyampholyte-modified microspheres as bio-lubricants attenuate osteoarthritis, Small 16 (44) (2020), e2004519.
[37] Y. Xu, Y. Li, Q. Chen, L. Fu, L. Tao, Y. Wei, Injectable and self-healing chitosan hydrogel based on imine bonds: design and therapeutic applications, Int. J. Mol. Sci. 19 (8) (2018).
[38] T. Subongkot, Combined effect of sonophoresis and a microemulsion on the dermal delivery of celecoxib, Drug Deliv. 27 (1) (2020) 1087–1093.
[39] E. Moghimipour, A. Salami, M. Monjezi, Formulation and evaluation of liposomes for transdermal delivery of celecoxib, Jundishapur J. Nat. Pharm. Prod. 10 (1) (2015), e17653.
[40] J.R. Yu, M. Janssen, B.J. Liang, H.C. Huang, J.P. Fisher, A liposome/gelatin methacrylate nanocomposite hydrogel system for delivery of stromal cell-derived factor-1α and stimulation of cell migration, Acta Biomater. 108 (2020) 67–76.
[41] R. Cheng, T. Xin, L. Liu, F. Wang, T. Ye, L. Deng, W. Cui, A "three-in-one" injectable hydrogel platform with osteogenesis, angiogenesis and antibacterial for guiding bone regeneration, Appl Mater Today 20 (2020) 100763.
[42] J.M. Graham, B.P. Ayati, L. Ding, P.S. Ramakrishnan, J.A. Martin, Reaction-diffusion-delay model for EPO/TNF-α interaction in articular cartilage lesion abatement, Biol. Direct 7 (2012) 9.
[43] L.J. Kang, J. Yoon, J.G. Rho, H.S. Han, S. Lee, Y.S. Oh, H. Kim, E. Kim, S.J. Kim, Y. T. Lim, J.H. Park, W.K. Song, S. Yang, W. Kim, Self-assembled hyaluronic acid nanoparticles for osteoarthritis treatment, Biomaterials 275 (2021) 120967.
[44] D. Heinegård, T. Saxne, The role of the cartilage matrix in osteoarthritis, Nat. Rev. Rheumatol. 7 (1) (2011) 50–56.
[45] L. Xing, D. Chen, B.F. Boyce, Mice deficient in NF-κB p50 and p52 or RANK have defective growth plate formation and post-natal dwarfism, Bone Res 1 (4) (2013) 336–345.
[46] Q. Hu, M. Ecker, Overview of MMP-13 as a promising target for the treatment of osteoarthritis, Int. J. Mol. Sci. 22 (4) (2021).
[47] T. Wang, Y. Liu, Y. Wang, X. Huang, W. Zhao, Z. Zhao, Long non-coding RNA XIST promotes extracellular matrix degradation by functioning as a competing endogenous RNA of miR-1277-5p in osteoarthritis, Int. J. Mol. Med. 44 (2) (2019) 630–642.
[48] X. Zhang, S. Koo, J.H. Kim, X. Huang, N. Kong, L. Zhang, J. Zhou, J. Xue, M. B. Harris, W. Tao, J.S. Kim, Nanoscale materials-based platforms for the treatment of bone-related diseases, Matter 4 (9) (2021) 2727–2764.
[49] S. Thysen, F.P. Luyten, R.J. Lories, Targets, models and challenges in osteoarthritis research, Dis Model Mech 8 (1) (2015) 17–30.
[50] M.T. Nieminen, V. Casula, M.T. Nevalainen, S. Saarakkala, Osteoarthritis year in review 2018: imaging, Osteoarthritis Cartilage 27 (3) (2019) 401–411.
[51] T. Paixao, M.D. DiFranco, R. Ljuhar, D. Ljuhar, C. Goetz, Z. Bertalan, H.P. Dimai, S. Nehrer, A novel quantitative metric for joint space width: data from the Osteoarthritis Initiative (OAI), Osteoarthritis Cartilage 28 (8) (2020) 1055–1061.
[52] L. Lieben, Osteoarthritis: osteophyte formation involves PAR2, Nat. Rev. Rheumatol. 12 (2) (2016) 70–71.
[53] P.M. van der Kraan, W.B. van den Berg, Osteophytes: relevance and biology, Osteoarthritis Cartilage 15 (3) (2007) 237–244.
[54] H. Wang, W.J. Zhang, J.H. Gao, J.R. Liu, Z.Y. Liu, B.Q. Xia, X.L. Fan, C.Z. Li, A. R. Qian, Global gene expression profiling of blast lung injury of goats exposed to shock wave, Chin. J. Traumatol. 23 (5) (2020) 249–257.
[55] H. Chen, T. Sun, Y. Yan, X. Ji, Y. Sun, X. Zhao, J. Qi, W. Cui, L. Deng, H. Zhang, Cartilage matrix-inspired biomimetic superlubricated nanospheres for treatment of osteoarthritis, Biomaterials 242 (2020) 119931.
[56] H. Tsushima, K. Okazaki, M. Hayashida, T. Ushijima, Y. Iwamoto, CCAAT/enhancer binding protein β regulates expression of matrix metalloproteinase-3 in arthritis, Ann. Rheum. Dis. 71 (1) (2012) 99–107.
[57] Z. Xu, T. Ke, Y. Zhang, L. Guo, F. Chen, W. He, Danshensu inhibits the IL-1β-induced inflammatory response in chondrocytes and osteoarthritis possibly via suppressing NF-κB signaling pathway, Mol. Med. 27 (1) (2021) 80.
[58] J. Zhou, Z. Zhang, J. Joseph, X. Zhang, B.E. Ferdows, D.N. Patel, W. Chen, G. Banfi, R. Molinaro, D. Cosco, N. Kong, N. Joshi, O.C. Farokhzad, C. Corbo, W. Tao, Biomaterials and nanomedicine for bone regeneration: progress and future prospects, Explorations 1 (2) (2021) 20210011.
[59] P.F. Han, L. Wei, Z.Q. Duan, Z.L. Zhang, T.Y. Chen, J.G. Lu, R.P. Zhao, X.M. Cao, P. C. Li, Z. Lv, X.C. Wei, Contribution of IL-1β, 6 and TNF-α to the form of post-traumatic osteoarthritis induced by "idealized" anterior cruciate ligament reconstruction in a porcine model, Int. Immunopharm. 65 (2018) 212–220.
[60] K. Aytekin, M. Uysal, G.G. Şahiner, M. Danışman, O. Baş, S. Takır, Z. Coşkun, E. Akdeniz, C.Z. Esenyel, Evaluation of different intraarticular injection volumes to assess optimum efficient amount; an experimental study in rat knee joints, J. Pharmacol. Toxicol. Methods 101 (2020) 106658.
[61] E. Teeple, K.A. Elsaid, G.D. Jay, L. Zhang, G.J. Badger, M. Akelman, T.F. Bliss, B. C. Fleming, Effects of supplemental intra-articular lubricin and hyaluronic acid on the progression of posttraumatic arthritis in the anterior cruciate ligament-deficient rat knee, Am. J. Sports Med. 39 (1) (2011) 164–172.
[62] S.J. Moon, Y.J. Woo, J.H. Jeong, M.K. Park, H.J. Oh, J.S. Park, E.K. Kim, M.L. Cho, S.H. Park, H.Y. Kim, J.K. Min, Rebamipide attenuates pain severity and cartilage degeneration in a rat model of osteoarthritis by downregulating oxidative damage and catabolic activity in chondrocytes, Osteoarthritis Cartilage 20 (11) (2012) 1426–1438.